Evidence of Polarization-type Potential-Induced Degradation (PID-p) in the Field and Investigation of the Recovery Mechanism on Bifacial *p*-PERC Modules

Cecile Molto[1], Dylan J. Colvin[1], Ryan Smith[2], Peter Hacke[3], Fang Li[4], Govindasamy Tamizhmani[4], Jaewon Oh[5], Halima Jahan[5], and Hubert Seigneur[1]

1. Florida Solar Energy Center – University of Central Florida, Cocoa, FL, 32922, USA
2. Pordis LLC, Austin, TX, 78729, USA
3. National Renewable Energy Laboratory, Golden, CO, 80401, USA
4. Photovoltaic Reliability Laboratory – Arizona State University, Mesa, AZ, 85212, USA
5. University of North Carolina at Charlotte, Charlotte, NC, 28223, USA.

Corresponding Author Email Address: cecile.molto@ucf.edu

Keywords: photovoltaics, potential-induced degradation, recovery, outdoor testing

Abstract: This study investigates the polarization-type Potential-Induced Degradation (PID-p) of bifacial glass/glass *p*-type Passivated Emitter Rear Contact (*p*-PERC) modules in the field and their recovery behavior. Modules were installed with three mounting configurations providing different albedo conditions. System voltage (-600 V, -1500 V, +1500 V) was applied to the cell circuits, with respect to the grounded module frames. No degradation was observed for positively-biased modules but PID-p was identified on the rear side when cells are negatively-biased, with maximum power dropping during the first days and stabilizing at values up to 8% loss. Electroluminescence images revealed a variation of the cells' PID-p suscepti-bility within a module. Three parameters were shown to impact the degradation rate: rear albedo light, voltage, and wetness conditions. Degraded modules were recovered either by: 1) a positive bias (+1500 V), 2) outdoor illumination with the front side facing sun, 3) outdoor illumination with the rear side facing sun, or 4) dark storage. A recovery pattern was identified with *I-V* parameters decreasing to a local min-imum before increasing to full recovery. The proposed mechanism is based on the band bending at the rear *p*-type Si/AlO_x/SiN_x interface, going from inversion to depletion and accumulation states. Full recovery was achieved in: 2 to 7 hours for the modules recovered with the rear side facing sun; 4 to 8 nights for the modules positively-biased at night; 10 to 20 days for the modules with the front side facing sun. Dark storage showed slower recovery rates as *I-V* parameters were not improv-ing even after one month. The recovery rates were correlated with the net Coulombs transferred during the preceding PID stress: when more Coulombs are transferred during the degradation, the extent of degradation is greater, leading to slower recov-ery rates.

1 Introduction

In the last few years, polarization-type Potential-Induced Degradation (PID-p) has been increasingly studied as it can affect emerging technologies, such as Passivated Emitter Rear Totally diffused (PERT), Tunnel Oxide Passivated Contact (TOPcon) and bifacial Passivated Emitter Rear Contact (PERC) modules [1–14]. While a brief state of the art on PID-p is given below, the reader can refer to the following review paper for more details [1].

PID-p studies, mainly performed indoors, enabled the identification of important aspects of the degradation mechanism that involve the accumulation of charged species in the passivation layers. When cells are positively-biased, it is suggested that positive charges are pushed away from the cells, leav-ing behind negative charges in the passivation layers that increase surface recombination velocity (SRV) of minority carrier holes at *n*-doped silicon (Si) surfaces[15]. This case has been less studied and the mechanism have not been demonstrated yet. For *p*-type Si, when cells are negatively-biased, an electric field directed towards the cells is created, leading to the accumulation of pos-itive charges in the passivation layers increasing the SRV of minority carrier electrons at the surfaces. Sodium ions (Na^+) contribute to the degradation by migrating from the glass to the dielectric layers but they are not the only species involved, as PID-p can occur within minutes (such that Na^+ ions do not have the time to diffuse to the passivation layers) and even in the absence of Na^+ ions. The role of K-centers present in the SiN_x layer was further demon-strated [4, 16]. A K-center is a dangling bond of Si atoms to three N atoms and it can be electrically neutral, negative, or positive (K_0, K^+, K^-). The electric field created when cells are negatively-biased can effectively change the K-centers polarity from neutral or negative into positive. The combined effect of Na^+ ions accumulation and K-center polarity change shifts the net charge in the passivation layers to a more positive value, inducing more SRV of the minority carriers. According to some authors, if enough positive charge develops in the passivation layers, the band bending at the Si surface is such that an inversion layer is created, reducing the SRV [11, 17] but this effect is not always observed. The properties of the passivation layers and encapsulant play a crucial role in the PID-p susceptibility [11, 13, 18–21]. Also, some stud-ies report a preventive effect of light on PID-p [2, 10, 11, 19, 22–25]: through UV-light absorption in the 300–390 nm wavelength range, the conductivity of the SiN_x layer can be increased, allowing the accumulated charges to dissi-pate. This effect is not always observed but happens more likely with an AlO_x layer rather than a SiO_x layer under the SiN_x layer [22]. As SiO_2 layers gen-erally have an higher resistivity than AlO_x layers, they will tend to prevent positive charge dissipation [16]. However, cells with an AlO_x/SiN_x stack might not show this effect depending on the manufacturing process [22]. PID-p can often, but not always, be recovered under light, reverse bias or dark storage [5, 11, 17, 26], but few studies have investigated the recovery mechanism, espe-cially in the field. There is a lack of outdoor studies investigating both the degradation and the recovery mechanism of PID-p.

This work provides useful data on commercially-available bifacial glass/-glass *p*-PERC modules affected by PID-p in the field under various voltages and albedo conditions. It is also the first of its kind to investigate the recovery of PID-p in the field. Four different recovery conditions are examined: 1) posi-tive bias recovery at night, 2) outdoor light-recovery with the front side facing sun, 3) outdoor light-recovery with the rear side facing sun, and 4) dark stor-age. The dark storage recovery is relevant to replicate how modules in the field will behave at night. The outdoor light-recovery results will enable assessment of the impact of light during power plant maintenance events for instance. The positive bias recovery will inform on the efficiency of this preventive solution. A recovery mechanism is proposed along with a discussion on the recovery rate as a function of the recovery method and the conditions the module was degraded. These results will serve the PV community to better understand how PID-p occurs in operating conditions, help differentiate PID-p from other degradation mechanisms that lead to reduced minority carrier lifetime, develop predictive models, develop PID-p preventive solutions, and improve standard accelerated PID-p tests to accurately reproduce what happens in the field.

2 Methods

2.1 Materials

40 framed bifacial glass/glass *p*-PERC modules (420 W nominal) with ethylene-vinyl acetate (EVA) encapsulant on both sides were purchased from one manufacturer. The rear passivation stack was identified by transmission electron microcopy and consists of a thin (≈ 10 nm) AlO_x with a SiN_x of about 70 nm. In a previous work [27], the PID-p susceptibility was evidenced in envi-ronmental chamber testing using the Al foil method of IEC TS 62804-1:2015, "Test methods for the detection of potential-induced degradation – Crystalline silicon" [28]. When cells are negatively-biased with respect to the grounded frame, PID-p is observed on the rear side with no shunting-type PID on the front side. When cells are positively-biased, a small degradation attributed to PID-p is observed on the front side. Results are detailed in reference [27], where the modules used in the present work are designated as "MB" in that reference.

2.2 High-voltage (HV) testbed

The HV testbed located at the Florida Solar Energy Center (FSEC) (humid subtropical climate) introduced in [29, 30] is designed to test modules in out-door conditions while applying voltages in the range of -3500 V to +1500 V. Four mounting racks can each accommodate 10 modules and rolling structures placed under each rack provide various albedo conditions (Figure 1). Each module is facing sun and slightly inclined with 3° tilt angle so that water does not pool, which results in a relatively stressful but realistic installation for the occurrence of PID. This same tilt angle was used for all our module to provide comparable wetting condition, in particular when it is raining. The different mounting racks are designed as follows:

- Simulated ground mounting (SIM ground) - 1 Rack: It mimics the albedo conditions of modules mounted in the field with grass growing tall enough to touch the rear side of the modules (which is a very common occurrence in solar power plants). Modules are mounted 30 cm above a rolling structure containing soil and grass,
- Simulated residential rooftop (SIM roof) - 1 Rack: It mimics the albedo conditions of modules on a typical flat commercial roof in America. Modules are mounted 30 cm standoff over a rolling structure covered by a black roofing material known as ethylene propylene diene monomer (EPDM) membrane,
- Open Racks - 2 Racks: They mimic the albedo conditions of modules mounted 2 meters above the ground (no structure placed under the modules).

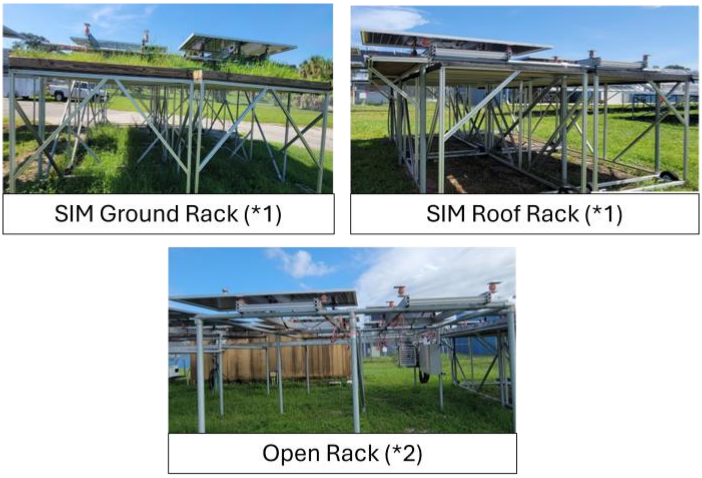

Fig. 1: Pictures of the three mounting configurations on the HV testbed (4 racks in total).

These three mounting configurations were chosen to mimic real-world scenarios while providing significantly different albedo light conditions (see Figure). The objective was to observe differences in the PID-p degradation or recov-ery rate on the different mounting configurations and establish a potential relationship between PID-p degradation or recovery rate and albedo light. It is worth mentioning that translating the results of this study to real-world case scenarios has some limitations. The 3° tilt angle used in this study differs from what is generally used in real world open racks scenarios (25-45°). As the albedo light received on the backside of the module depends on the module tilt angle [31], it will be necessary to estimate the increase of albedo dose received by the module for higher tilt angle. Also, other parameters such as the temperature and humidity might have an impact on the PID-p degradation or recovery rate and are not investigated in this paper. Moreover, using a different cell technology or module construction might give different results even if the environmental parameters and mounting configuration are strictly the same.

A dedicated shielded leakage current cable is fitted to each module frame. On each mounting rack, there is one control unbiased module and 8 modules out of 10 modules can be *I-V* traced. A meteorological station measures the wind speed and direction, the ambient temperature and humidity, and the precipitation. Sensors are installed on the HV testbed: 1) leaf wetness sensor, 2) plane-of-array (POA) UV sensor, 3) POA irradiance sensor (Licor POA), 4) irradiance sensors placed under each rack to measure the albedo irradiance (Licor albedo), 5) UV sensors placed under each rack to measure the UV albedo, 6) thermocouples on the rear side of some modules.

2.3 Outdoor data filtering and *I-V* correction procedure

Any data impacted by maintenance or equipment failure was removed from the analysis. A sky stability filter was applied to the *I-V* data such as the standard deviation of the Licor POA one minute before and 30 seconds after an *I-V* trace did not exceed 3 W/m^2. Correcting the *I-V* to Standard Testing Conditions (STC; AM1.5G, 25°C, 1000 W/m^2) can induce significant errors when the module is degrading [32], in particular for low irradiance *I-V* traces where the smaller output of the module makes it more susceptible to the impact of shunt resistance, temperature variations, and spectral discrepancies [33].

Therefore, maximum power (P_{max}), short-circuit current (I_{SC}) and open-circuit voltage (V_{OC}) were normalized to the closest respective unbiased control module ($P_{max\ control}$, $I_{SC\ control}$ and $V_{OC\ control}$) using equations 1,2, 3, respectively. This way, only the degradation due to high voltage will be reflected in the corrected *I-V* parameters. As irradiance conditions might slightly change between the time a module is *I-V* traced and the time its control is *I-V* traced, the difference of Licor POA irradiance (G_{POA}) between a module and its control was considered to correct P_{max} and I_{SC}. The normalization did not account for the temperature as there was no significant temperature difference between biased and unbiased modules. *I-V* traces measured more than 3 minutes apart from a control module were not considered as important change of the environmental conditions could happen and lead to significant error of the *I-V* correction.

$$P_{max\ normalized} = \frac{P_{max}}{P_{max\ control}} \times \frac{G_{POA}}{G_{POA_{control}}} \quad (1)$$

$$I = \frac{I_{SC}}{} \times \frac{G_{POA}}{} \quad (2)$$

$_{SC\ normalized}$ $I_{SC\ control}$ $G_{POA\ control}$

$$V_{OC\ normalized} = \frac{V_{OC}}{V_{OC\ control}} \quad (3)$$

2.4 Indoor characterization

Indoor illuminated *I-V* were measured with a Sinton FMT-350 and electroluminescence (EL) imaging was performed using a modified consumer DSLR-CMOS camera with a 950 nm longpass filter. Each side of the modules was measured individually by blocking the opposite side (*e.g.*, front side measurements are taken with the rear side blocked to minimize rear reflection of the measurement apparatus).

2.5 PID degradation and recovery protocols

Two rounds of outdoor degradation were performed to test various high voltages. Modules degraded in the first round of exposure (Round 1) were used for the recovery experiments. To avoid any light-induced recovery during removal and reinstallation of the modules for indoor measurement, a cardboard sheet was secured on the rear side when voltage was turned off and transport from the field to the lab was done immediately after each module was uninstalled with the rear side facing down. In the next sections, we describe the two degra-dation rounds performed in sequential years followed by a description of the recovery testing.

2.5.1 Outdoor degradation: Round 1 and Round 2

The first round (Round 1) of degradation was performed on 20 modules (5 per rack) from June, 9th, 2023 to May 2024. The module layout is given in Figure 2. -1500 V was applied to the cells on the SIM ground (Rack A), Open Rack B and SIM roof (Rack E). On the Open Rack D, +1500 V was applied to the cells. All frames were connected to ground via a current-sensing resistor circuit and one control module (unbiased) was installed per rack. After 3 months of light soaking with the modules connected to load resistors, HV was applied starting June, 9th, 2023 during the day and turned off at night. All modules except M7, M17, M31 and M41 were *I-V* traced. Due to equipment complications, the negative voltage on the SIM roof was applied with an 8-week delay and the *I-V* capability for M35 and M43 was lost. Indoor *I-V* and EL were performed in approximately 3-month intervals.

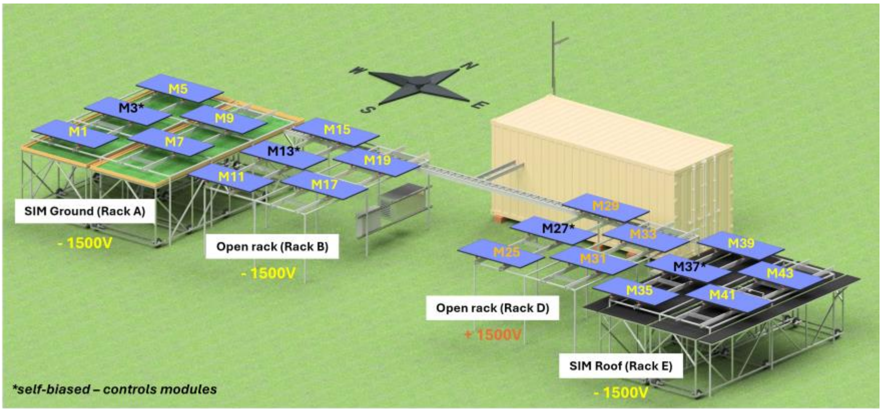

Fig. 2: Module layout for Round 1 outdoor degradation.

The second round (Round 2) of outdoor degradation was performed on another batch of 20 modules to test lower high-voltages. The module layout is given in Figure 3. -600 V was applied to the cells on the SIM ground (Rack A), Open Rack D and SIM roof (Rack E). The Open Rack B was stressed with the same voltage (-1500 V) and mounting configuration as Round 1. Based on Round 1 results, testing was reduced to 3 weeks (September, 27th, 2024 to October 7th, 2024). All frames were grounded and one control module (unbiased) was installed per rack. Modules were light-soaked before applying the HV during the day (turned off at night). All modules except M4, M6, M14, M16, M28 and M38 were *I-V* traced.

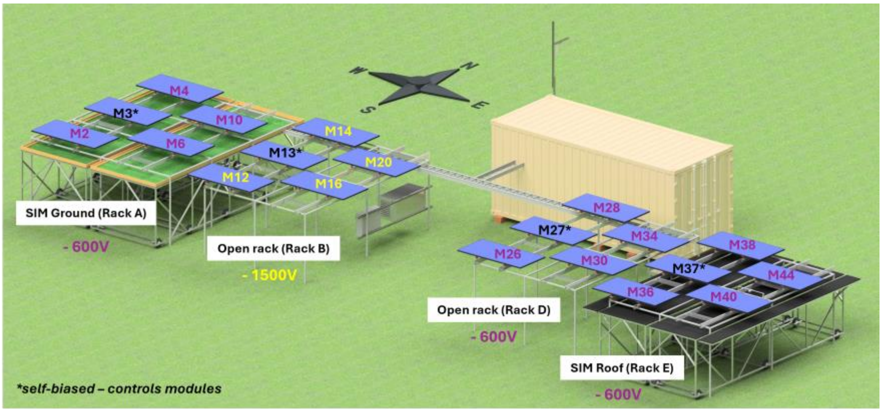

Fig. 3: Module layout for Round 2 outdoor testing.

2.5.2 Recovery experiments

PID-p degraded modules from Round 1 were used to investigate four recovery methods. Indoor *I-V* and EL measurements were done at the end of Round 1 and, for each rack, one module underwent one of the four recovery experiment summarized in Figure 4:

- Dark storage recovery (M7, M17, M41): modules were kept in the laboratory with indoor *I-V* and EL performed once a week;
- Nighttime positive bias recovery (M1, M11, M35): modules were reinstalled in the field on Open Rack D with +1500 V applied at night. During the day, the modules' rear side was covered to avoid light-induced recovery. Indoor *I-V* and EL were performed every morning;
- Light-induced recovery with the front side facing the sun (M9, M19, M43): modules were reinstalled in the field with the front side facing sun with no applied voltage bias. Outdoor *I-V* tracing was performed every 5 minutes;
- Light-induced recovery with the rear side facing the sun (M5, M15, M39): modules were reinstalled in the field with the rear side facing sun with no applied voltage bias. Outdoor *I-V* tracing was performed every 5 minutes.

The module layout for the recovery experiment is given in Figure 5. For the light-induced recovery experiments, the modules were installed at the same location used for degradation, except for the SIM Roof modules because no *I-V* tracing was possible on this Rack at the time, so M39 and M43 were recovered on the Open Rack B. Control modules M3 and M13 were reinstalled to enable correction of P_{max}, I_{SC} and V_{OC} of the recovering modules using equations 1,2 and 3.

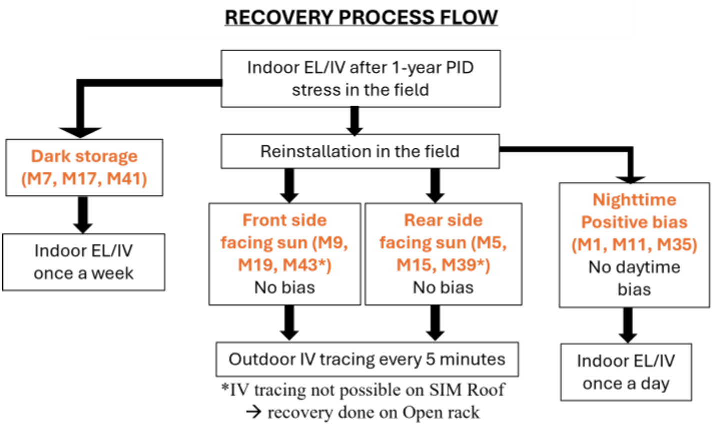

Fig. 4: Process flow of the four recovery experiment performed on modules affected by PID-p in Round 1.

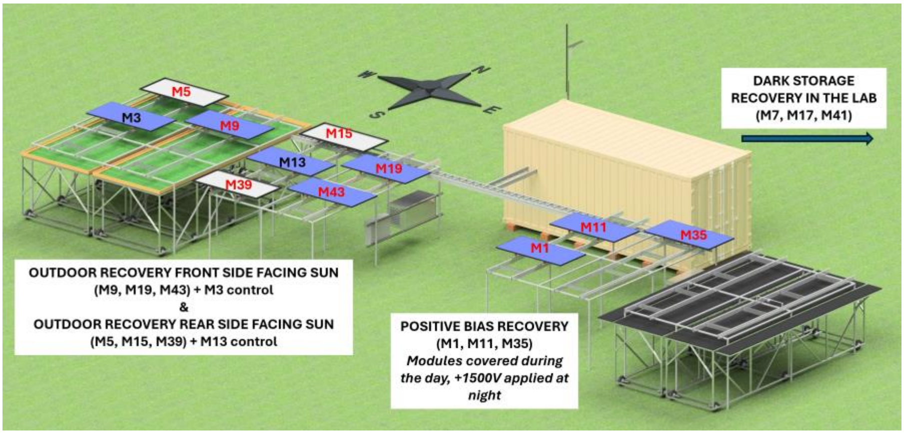

Fig. 5: Modules layout for the recovery experiments on modules affected by PID-p in Round 1.

3 Results and Discussion

3.1 Evidence of PID-p in the field

3.1.1 Round 1 outdoor degradation: impact of light on PID-p

Outdoor *I-V* data were normalized to their respective control module (see section 2.3) and the daily median value of $P_{max\ normalized}$ over time is given in Figure 6 for the negatively-biased modules on SIM Ground, Open Rack B and SIM roof. No degradation was observed on the positively-biased modules on Open Rack D (data not shown here). The daily median $I_{SC\ normalized}$ and $V_{OC\ normalized}$ over time are shown in supporting information SI.1 and SI.2. Modules were uninstalled for indoor *I-V* and EL on 22-Aug-2023, 05-Oct-2023, 16-Jan-2024, and 17-Apr-2024 which corresponds to 10, 16, 31, and 44 weeks of system voltage application for the modules on SIM ground and Open Rack B. For the SIM roof rack, this corresponds to 1, 7, 22, and 35 weeks of system voltage application. Corresponding P_{max} are displayed in Figure 7 while I_{SC} and V_{OC} can be found in the supporting information sections SI.3 and SI.4, respectively. EL images of one representative module per rack are shown in Figure 8.

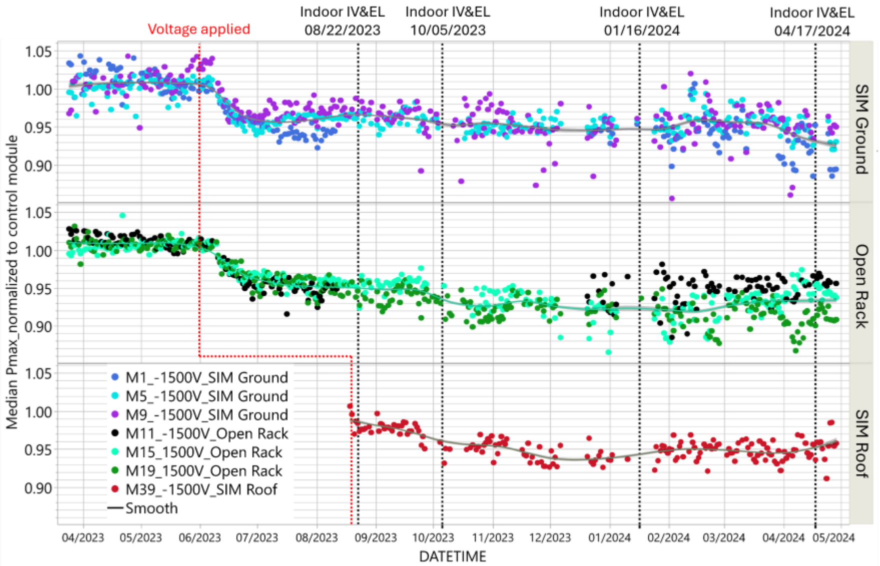

Fig. 6: Outdoor *I-V* $P_{max\ normalized}$ over time during Round 1 degradation for negatively-biased modules on SIM Ground, Open Rack B and SIM Roof (daily median).

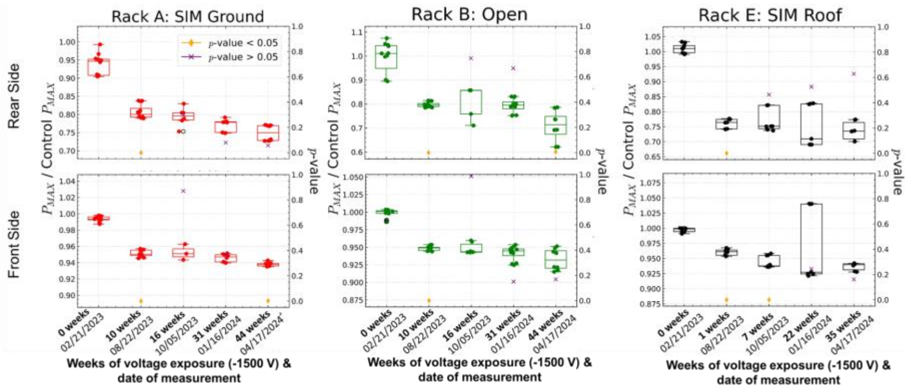

Fig. 7: Indoor *I-V* P_{max} data during Round 1 degradation for negatively-biased modules on SIM Ground, Open Rack B and SIM Roof. Each row is labeled based on which side of the module is measured (front or rear). Each of these parameters is normalized to the values of the respective rack control modules. *p*-values between successive measurements are indicated on the right scale.

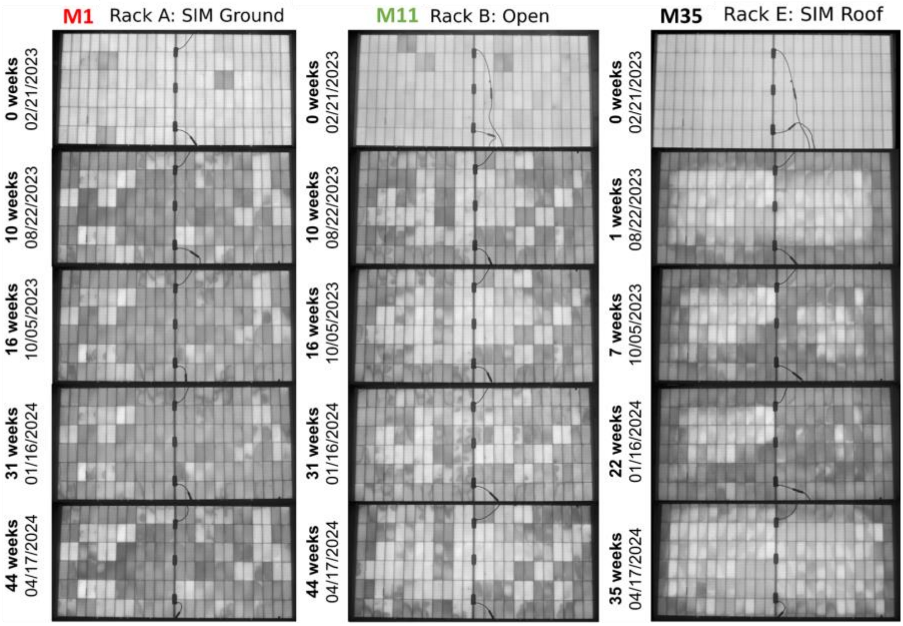

Fig. 8: EL images for one representative module per rack during Round 1. Images shown are taken at nameplate I_{SC} on the rear side of the module. The image for rack E at 0 weeks of bias is at 70% nameplate I_{SC} due to poor image quality at higher currents on that date.

As shown in Figure 6, P_{max} quickly drops after -1500 V is applied and stabilizes in the range of 5 to 8 % loss after about 2 to 3 weeks. The same trends are observed for I_{SC} and V_{OC} with a stronger impact on I_{SC}, which is typical of PID-p [1]. Indoor data (Figure 7) (when flashing the front side) show the same level of degradation compared to what is observed outdoors. Performance losses are more pronounced when flashing the rear side of the module where the degradation happens. The EL images in Figure 8 display a checkerboard pattern of cells' brightness indicating a variability of the PID-p susceptibility for the different cells of the module.

For each mounting rack, the mean P_{max} degradation rate of the four biased modules (% P_{max} loss/day) during the P_{max} dropping phase (first 10 days) was calculated using a linear regression. Results are reported in Table 1 along with the mean daily Licor albedo dose (Wh/m^2/day) for the same period. We notice a slower degradation rate with greater albedo light doses: modules on the Open Rack receive more albedo light and degrade more slowly than the one on the SIM Ground, which degrade more slowly than the modules on the SIM Roof, having received the least albedo light. This confirms the preventive effect of light on PID-p in the field. Round 1 data were used to develop a sigmoidal model describing the module power as a function of charge incoming from the negative voltage applied and countered by dissipation from incident irradiation. This model is presented in reference [34].

Table 1: P_{max} degradation rate (mean value of 4 modules) as a function of the mean daily Licor albedo dose during the first 10 days of voltage in Round 1.

Mounting configuration	Mean Licor Albedo dose ($Wh/m^2/day$)	Mean degradation rate ($\%P_{max}$ loss/day)
SIM Roof (-1500 V)	26.46	-7.612×10^{-1}
SIM Ground (-1500 V)	359.07	-3.525×10^{-1}
Open Rack (-1500 V)	710.56	-2.497×10^{-1}

A slight seasonal effect was noticed with lower median value of $P_{max\ normalized}$ between mid-September and April (see Figure 6). The Licor and UV albedo dose per day during Round 1 are given in Figure 9 and support-ing information SI.5, respectively. They seem to mirror the $P_{max\ normalized}$ behavior with a dip between mid-September and April, suggesting that lower irradiance conditions in fall and winter are responsible for slightly greater PID-p.

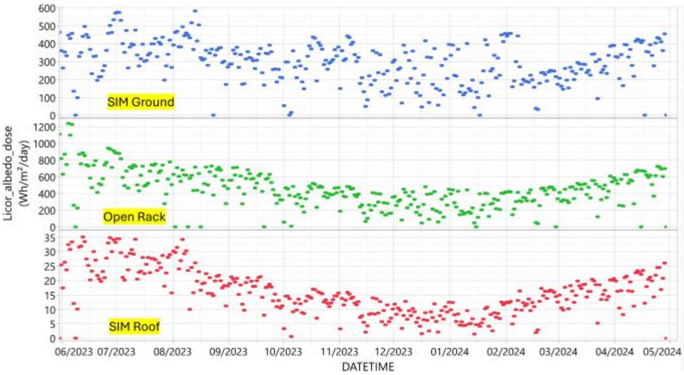

Fig. 9: Evolution of the Licor albedo dose ($Wh/m^2/day$) for each mounting configuration during Round 1 degradation.

3.1.2 Round 2 outdoor degradation: impact of voltage on PID-p

Outdoor *I-V* data were normalized to their respective control module and the hourly median value of $P_{max\ normalized}$ over time is given in Figure 10 for the modules stressed at -600 V on SIM Ground, Open Rack D and SIM roof. Similarly, Figure 11 compares modules stressed on the Open Rack B (-1500

V) and Open Rack D (-600 V). The corresponding graph for hourly median $I_{SC\ normalized}$ are given in supporting information SI.6 and SI.7. In Table 2, the mean daily Licor albedo dose, the mean daily UV albedo dose, and the mean P_{max} degradation rate (%P_{max} loss/day) during the P_{max} dropping phase (first 3 days) are reported for each rack.

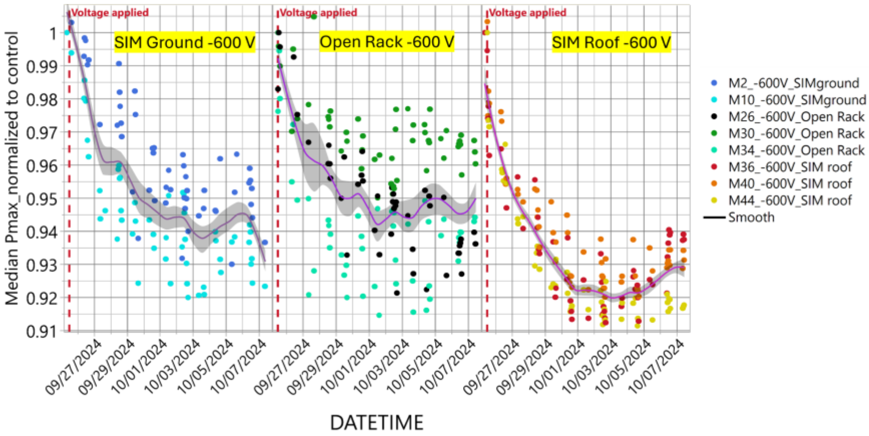

Fig. 10: Hourly median of outdoor *I-V* $P_{max\ normalized}$ over time during Round 2 degradation for the modules stressed at -600 V with different mount-ing configuration.

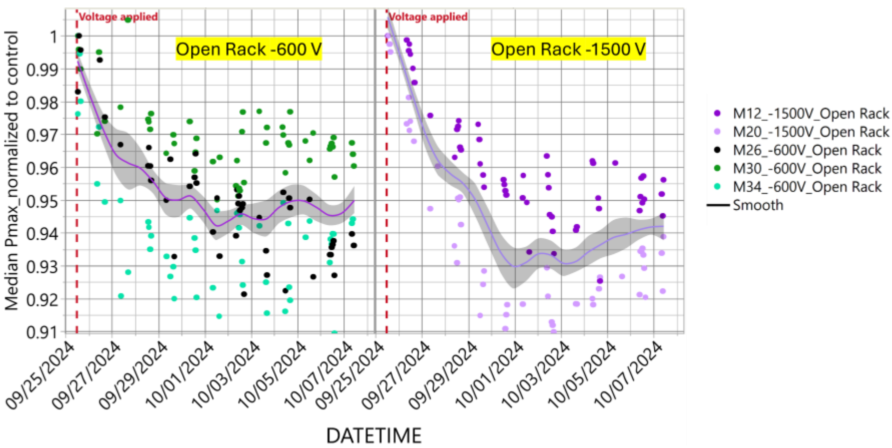

Fig. 11: Hourly median of $P_{max\ normalized}$ over time during Round 2 degra-dation for the modules stressed on Open Racks.

Table 2: P_{max} degradation rate (mean value of 4 modules) as a function of the mean daily Licor and UV albedo dose during for each mounting configuration during the first 3 days of stress in Round 2.

Mounting configuration	Mean daily Licor albedo dose ($Wh/m^2/day$)	Mean daily UV albedo dose ($Wh/m^2/day$)	Mean degradation rate (%P_{max} loss/day)
SIM Roof (-600 V)	10.69	0.044	-1.296
SIM Ground (-600 V)	158.17	0.046	-1.270
Open Rack (-600 V)	307.92	0.407	-1.019
Open Rack (-1500 V)	307.92	0.407	-1.486

P_{max} in Round 2 quickly drops when a negative voltage is applied and stabilizes after 3-4 days with P_{max} loss up to 8%. The mean P_{max} degradation rates in Round 2 (Table 2) are almost the same for SIM Ground and SIM Roof stressed at -600 V. While the mean daily Licor albedo dose was significantly different between SIM Ground and SIM Roof, the mean daily UV albedo doses were similar. This suggests that the UV albedo conditions correlate better with the PID-p degradation rate than the Licor albedo conditions. As the UV component of light is responsible for the PID-p preventive effect[22], these results make sense. With a mean daily UV albedo dose ≈ 10 times greater on the Open Rack stressed at the same voltage, the mean P_{max} degradation rate slows down by a factor of ≈ 1.27, confirming the impact of the mounting configuration on PID-p as observed in Round 1. When comparing the Open Racks at -1500 V and -600 V in Round 2 (Table 2), the mean P_{max} degradation rate is ≈ 1.45 times faster when the voltage is increased by a factor of 2.3. This highlights a greater impact of the voltage on the PID-p degradation rate than the UV-light.

3.1.3 Comparison Round 1 and Round 2 outdoor degradation: impact of modules' wetness on PID-p

To evaluate the underlying factors governing the Round 1 and Round 2 degradation rates, the wetness conditions measured by the leaf wetness sensor during the P_{max} degradation phases are given in supporting information SI.8 for both rounds. The percentage of wetness data reporting 'Dry' conditions was 36% in Round 1 (from 09-June-2023 to 19-June-2023) and 16% in Round 2 (from 26-Sep-2024 to 29-Sep-2024). Mean ambient temperature and %RH were similar (28.2 °C ± 3.6 and 69.5 % ± 14.6 in Round 1; 28.9 °C ± 1.86 and 78.0 % ± 11.7 in Round 2). During Round 1, the mean P_{max} degradation rate at -1500 V on the Open rack was -2.497 x 10^{-1} %P_{max} loss per day with a mean daily Licor sensor albedo dose of 711 $Wh/m^2/day$. During Round 2, the mean P_{max} degradation rate at same voltage and mounting configuration was -1.486 %P_{max} loss per day with a mean daily Licor sensor albedo dose of 308 $Wh/m^2/day$.

This represents a P_{max} degradation rate during the P_{max} dropping phase ≈ 6 times faster in Round 2 for a daily Licor albedo dose ≈ 2.3 times lower. A difference in irradiance conditions seems insufficient to explain the significantly faster degradation in Round 2. While the ambient temperature and %RH were similar, the wetness conditions in the first days of voltage application were significantly different with 2 times more readings of dry conditions in Round 1 based on the leaf wetness sensor. When modules are wet, the impact of voltage difference between the cells and ground potential extended over the surface of the module glass from the frame is more uniformly distributed, which is favorable for the occurrence of PID-p.

3.2 Identification of a PID-p recovery pattern

3.2.1 Outdoor light-induced recovery front side facing sun

Modules M9, M19 and M43 (degraded during Round 1 on SIM Ground, Open Rack B, and SIM Roof, respectively) were recovered under sunlight with the modules' front side facing the sun. The resulting $P_{max\ normalized}$ over time are given in Figure 12. The three modules show a similar recovery pattern where P_{max} first drops, reaches a local minimum and then increases until full recovery. M43 recovers the fastest (≈ 10 days), followed by M19 (≈ 17 days) and then M9 (≈ 20 days). M19 and M43 have a different recovery rate, even though they were both recovered on an Open Rack (meaning that they received the same amount of UV albedo light during recovery). This seems to indicate that the degradation history plays a role in the recovery rate. In the case of M9 recovered on the SIM Ground rack, a lower recovery rate is reported, which could be attributed to 1) the difference of degradation history with M19 and M43 and, 2) the lower UV albedo dose measured during recovery on the SIM Ground.

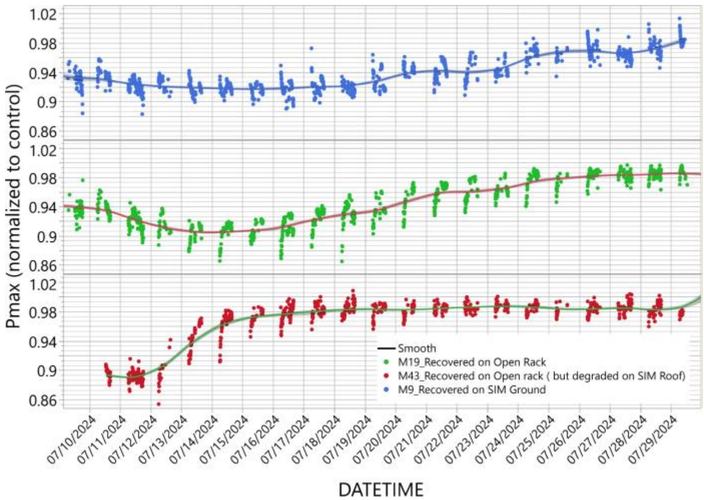

Fig. 12: $P_{max\ normalized}$ over time during outdoor light-recovery with front side facing sun on Round 1 degraded modules (M9, M19, M43).

A significant variation of $P_{max\ normalized}$ was observed over the day (see Figure 12) until modules fully recovered. A comparison of $P_{max\ normalized}$ at the beginning of M19 recovery with the corresponding Licor albedo values is shown in supporting information SI.9. A strong correlation is observed, suggesting a dependence of $P_{max\ normalized}$ on the irradiance conditions, which is unusual for P_{max} normalized to the control module. It has been reported that measured degradation (by either flashing the degraded or non-degraded side) associated with PID-p is greater when *I-V* flashing the module at low irradiance [11, 27]. This injection-level dependent behavior could be explained by the dependency of the effective SRV with the excess carrier concentration (*i.e.*, injection level), as demonstrated by Aberle *et al.* on *p*-type silicon samples [35]. Therefore, a greater difference of P_{max} between a PID-p degraded module and its control would be observed with lower albedo irradiance condition (i.e., in the early morning). Not only the irradiance intensity but also the associated solar spectrum could be involved in the phenomenon observed in Figure 12 as higher concentration of infrared wavelengths are often reported in the solar spectrum in the early morning. Further analysis would be need to explore this hypothesis. As the variation of $P_{max\ normalized}$ over the day reduces with the progression of the recovery, this behavior could be used to specifically detect PID-p in the field.

As shown in Figure 12, full outdoor recovery front side facing sun takes at least 10 days. This recovery method does not seem desirable in a real PV plant as disconnecting modules for such a long period would cause significant financial losses.

3.2.2 Outdoor light-induced recovery rear side facing sun

Modules M5, M15 and M39 (degraded during Round 1 on SIM Ground, Open Rack B and SIM Roof, respectively) were recovered under sunlight with the rear side facing the sun. Due to a rain event, modules were covered for two days with an opaque tarp for safety. $P_{max\ normalized}$ over time is given in Figure 13 (before the rain event) and Figure 14 (after the rain event). Here again, $P_{max\ normalized}$ first decreases, reaches a local minimum and then increases until full recovery. The slopes of the dropping and increasing phases are indi-cated on the graphs. The module that was degraded on the SIM Roof (M39) recovered the fastest and the one degraded on the SIM Ground (M5) recov-ered the slowest. For instance, $P_{max\ normalized}$ drops 2.6 times faster at the beginning of the recovery process for M39 compared to M5. As the modules are flipped with the degraded side (rear) facing sun, and as all racks have the same tilt angle, the amount of light involved in the recovery process will be the same whichever rack the modules are mounted on. The albedo light might vary but it is not impacting the recovery since it reaches the non-degraded (front) side. Consequently, differences in recovery speed can be attributed to the different degradation history of the modules.

This confirms the impact of the degradation history on the recovery rate as M5, M15 and M39 were degraded under different mounting configuration (see Figure 2) resulting in more albedo light for M15, followed by M5 and then M39. It is important to note that M39 was also stressed 8 weeks after the other modules, resulting in a shorter PID stress. Full recovery is obtained in a matter of hours: 2.5 hours for M39 originally mounted on the SIM Roof, 6 hours for M15, originally on the Open Rack and 9 hours for M5, originally on the SIM Ground (end of the experiment performed another day on M5 due to another rain event, data not shown here).

Recovering the PID-p impacted modules with the rear side facing sun gave promising results as full recovery can be achieved in a couple of hours. While it is not feasible to completely flip the modules on a real PV plant as we did in this study, modules on a tracking system could be tilted for a short period of time when the irradiance is high and angle of incidence is low.

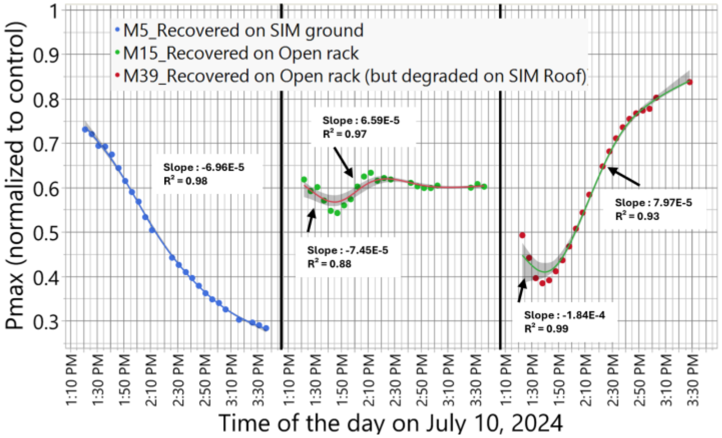

Fig. 13: $P_{max\ normalized}$ over time during outdoor light-recovery rear side facing sun of Round 1 degraded modules (M5, M15, M39) (before rain event).

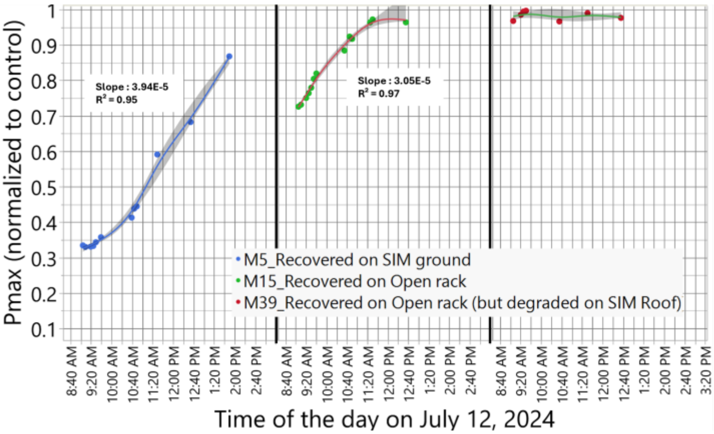

Fig. 14: $P_{max\ normalized}$ over time during outdoor light-recovery rear side facing sun of Round 1 degraded modules (M5, M15, M39) (after rain event).

3.2.3 Dark storage recovery

Modules M7, M17 and M41 (degraded during Round 1 on SIM Ground, Open Rack B and SIM Roof, respectively) were kept in the lab for 1 month. Weekly indoor *I-V* were performed and P_{max} values are reported in Figure 15. I_{SC}, V_{OC} and EL images are given in supporting information SI.10, SI.11 and SI.12. Here, the recovery rate is significantly slower: *I-V* parameters dropped and might have reached a local minimum but no significant increase is observed even after 1 month. EL images show a checkerboard pattern even if the cells' EL intensity changed, indicating that the recovery process is ongoing. These results confirm that PID-p recovery can occur without light but at a significantly slower rate than when light is used. Longer dark storage would be necessary to confirm the ability to fully recover and determine a recovery rate.

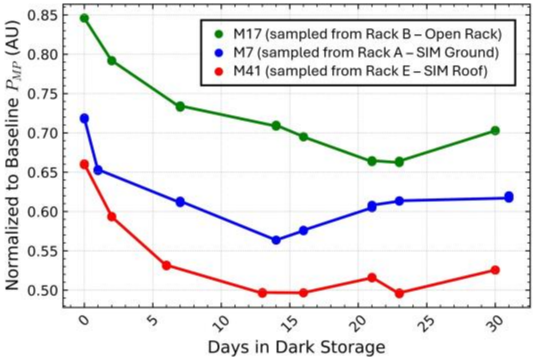

Fig. 15: Indoor *I-V* P_{max} data during dark storage recovery on Round 1 degraded modules (M7, M17, M41). P_{max} is obtained by flashing the modules' rear side and normalized to the baseline taken before degradation.

3.2.4 Nighttime positive bias recovery

Modules M1, M11 and M35 (degraded during Round 1 on SIM Ground, Open Rack B and SIM Roof, respectively) were recovered by applying a positive bias (+1500 V) at night. Indoor *I-V* were performed every morning and P_{max} are reported in Figure 16. I_{SC} and V_{OC} are given in supporting information SI.13 and SI.14. EL images are displayed in supporting information SI.15 for M1, SI.16 for M11 and SI.17 for M35. The same pattern as the other recovery experiments can be noticed: *I-V* parameters decrease, reach a local minimum, and increase until full recovery. After one night, all three modules show their P_{max} local minimum and this is characterized on the corresponding EL images by the highest number dark cells (high surface recombination). This indicates that even during recovery, the surface recombination losses first increase before being reduced. While the recovery conditions are the same for the three modules, M35 that was degraded on the SIM Roof is recovering the fastest and M1 that was degraded on the SIM Ground seems to recover the slowest. Full recovery occurs between ≈ 5 to 7 nights for all three modules as confirmed by the EL images.

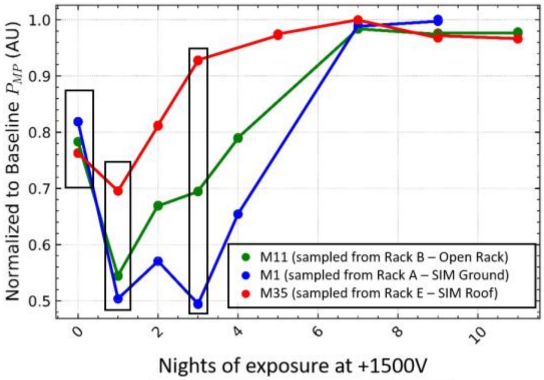

Fig. 16: Indoor *I-V* P_{max} data during positive bias recovery at night (+1500 V) on Round 1 degraded modules (M1, M11, M35). P_{max} is obtained by flashing the modules' rear side and normalized to the baseline taken before degradation. EL images of corresponding to the boxed data points are given in Figure 20.

3.3 Correlation between PID-p recovery rate and PID-p degradation history

All the recovery experiments performed have resulted in a faster recovery rate for the modules degraded on the SIM Roof, followed by the modules degraded on the Open Rack and then the modules degraded on the SIM Ground (except for dark storage recovery that was not long enough to determine the recovery rates). Since the modules degraded on the SIM Roof in Round 1 were stressed with few weeks delay, it is likely that fewer positive charges were accumulated on these modules. This possibility is examined further in Figure 17. For Each recovery experiment, $P_{max\ normalized}$ after a time of recovery corresponding to a certain extent of band bending at the rear surface (an index for the state of the module), is compared to the total net Coulombs transferred during Round 1 degradation. The recovery duration was chosen such as $P_{max\ normalized}$ were already increasing, which corresponds to 2.5 hours of rear side facing sun recovery, 10 days of front side facing sun recovery and 4 nights of positive bias recovery. It can be observed in Figure 17 that less Coulombs were transferred for the modules degraded on the SIM Roof, followed by the modules degraded on the Open Rack and then the modules degraded on the SIM Ground. For all three recovery experiment, smaller $P_{max\ normalized}$ (after the chosen time of recovery) are associated with more Coulombs transferred during Round 1 degradation. For instance, M35-M11-M1 were degraded in different conditions but recovered the same way (positive bias at night) and M35 having the least Coulombs transferred during the degradation recovers the fastest while M1 having the more Coulombs transferred during the degradation recovers the slowest.

When more Coulombs are transferred during PID stress, the recovery is slower which could be related to a greater extent of PID stress. A greater extent of PID-p on the SIM Ground compared to the Open Rack can be explained by lower albedo light reaching the backside of the modules. While the modules on the SIM Roof should have shown the greater extent of PID-p (lowest albedo light condition), the delayed voltage stress is responsible for the opposite trend observed: SIM roof modules had the least net Coulombs transferred during PID stress, leading to the fastest recovery rate.

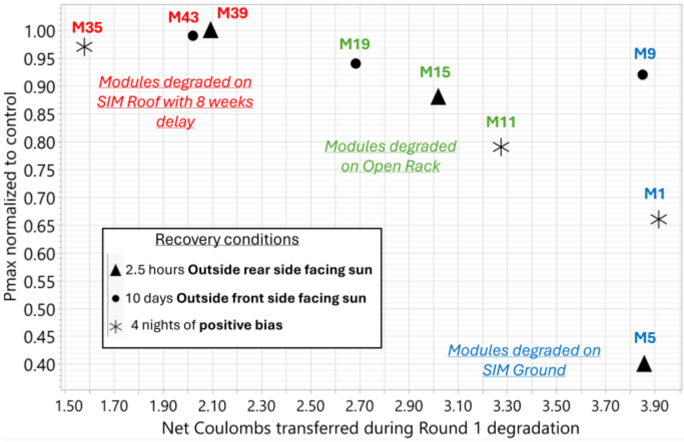

Fig. 17: $P_{max\ normalized}$ after a chosen period of recovery, such as P_{max} in the increasing phase, as a function of the net Coulombs transferred during Round 1 degradation.

3.4 Proposition of a PID-p degradation and recovery mechanism

Three band bending states can exist at the p-Si/AlO_x/SiN_x interface depending on the amount of positive charges accumulated in the dielectric stack: Accumulation (state A), depletion (state B) and inversion (state C). These states are schematized in Figure 18. They are associated with higher or lower SRV and will therefore impact differently the P_{max} and EL intensity as represented in Figure 19. While a depletion state is unfavorable for SRV, the inversion state actually tends to reduce SRV. P_{max} and the EL intensity are at their minimum value during the transition between depletion (state B) and inversion (state C).

PID-p degradation would consist of going from accumulation (state A) to depletion (state B) and eventually inversion (state C). The different states during PID-p are described below, assuming that the cells are negatively-biased respectively to the grounded frame:

- Accumulation: Before any stress, the fixed negative charges in the AlO_x layer repel the minority-carrier electrons from the Si surface and create an upward bending of the Si bands through a redistribution of majority-carrier holes that accumulate in the Space Charge Region (SCR). This results into an electric field ($\vec{E}_1$) also repelling minority-carrier electrons,
- Depletion: When positive charges accumulate in the passivation layers, the overall net charge in the passivation layers shifts to more positive values, reducing the ability to repel minority-carrier electrons. Meanwhile, the Si band bends downward as majority-carrier holes are depleted from the SCR, creating an electric field ($\vec{E}_2$) unfavorable to repel electrons. This state is induced by Na^+ accumulation and K-center polarity change into K^+. The further the depletion progresses, the more the SRV increases, resulting in a decrease of P_{max} and EL intensity,
- Inversion: Once enough positive charges are accumulated, the semiconductor Fermi level $E_{f,p}$ crosses the minority-carrier band E_c, leading to an accumulation of mobile minority-carriers at the surface. An electric field ($\vec{E}_3$) is created, repelling minority-carrier electrons from the Si surface and balances the effect of positively charged AlO_x/SiN_x stack. This results in an increase of P_{max} and EL intensity while progressing into the inversion (state C). Inversion is limited by the generation of minority-carriers and unlikely achieve SRV as low as in the accumulation state.

This mechanism implies that a local minimum for P_{max} is observed as schematized in Figure 19, which has been reported in some papers [11, 17] but not others [2, 5, 18]. P_{max} often decreases and stabilizes, which was the case in this work, and it is still not clear why a local minimum is not systematically observed during degradation.

Through the dissipation of the accumulated charges (out-diffusion of Na^+ ions and K^+ centers going back to their initial state), PID-p recovery occurs by going backwards from inversion to depletion and accumulation. The process is very slow in dark storage but can be accelerated by the application of a positive bias or by sunlight illumination. Direct illumination of the degraded side is the most effective method to recover the modules in a matter of few hours. It can be hypothesized that the direct illumination of the degraded side allows faster recovery than the application of a positive bias due to a different mechanism of positive charge dissipation. With a positive bias, positive charge would be drifted out of the passivation layers towards the encapsulant with an impact of the passivation layers' resistivity on the diffusion rate. A direct illumination of the degraded side would decrease the resistivity of the passivation layers stack, allowing a faster and lateral dissipation of the positive charges.

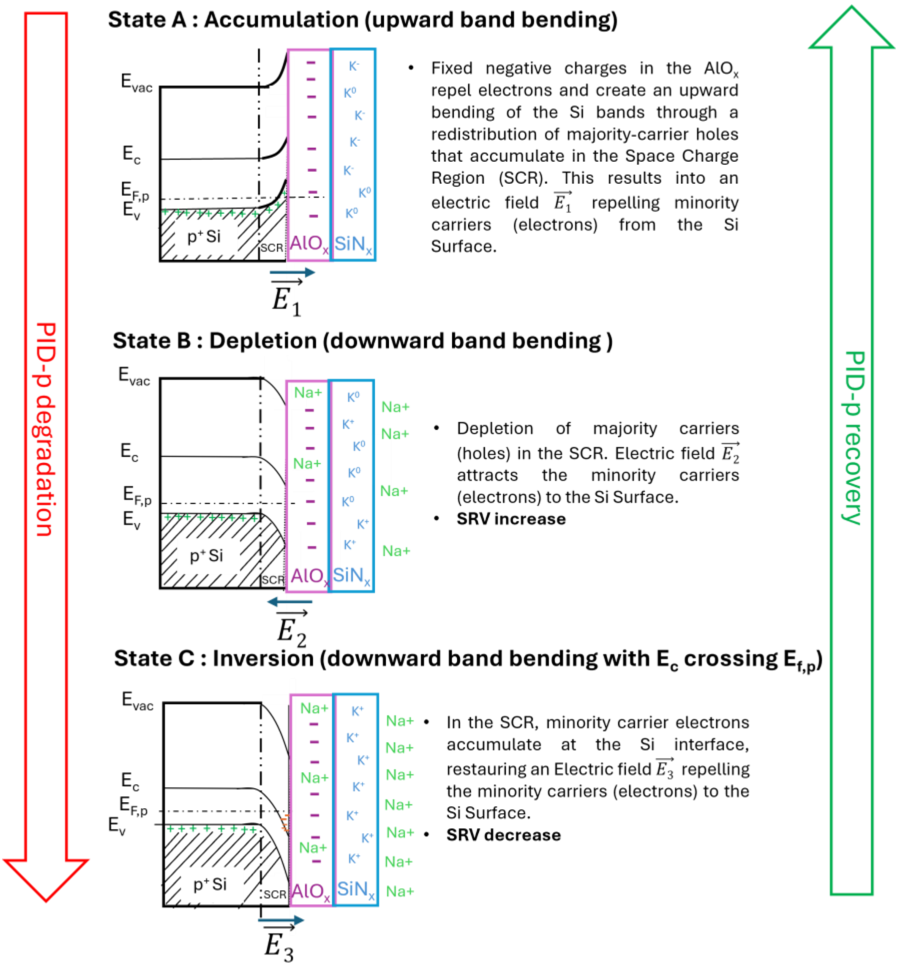

Fig. 18: Illustration of existing band bending states at the *p*-Si/AlO$_x$/SiN$_x$ interfaces during PID-p degradation and recovery processes (degradation under a negative bias applied to the cells, respectively to the grounded frame).

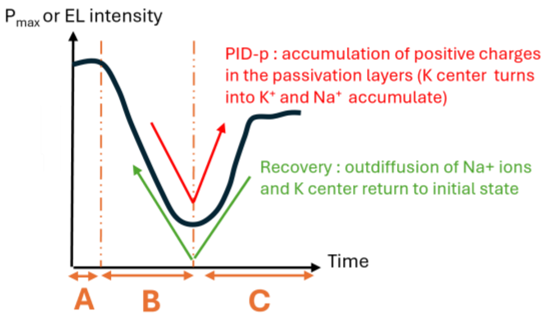

Fig. 19: Schematic representation of P_{max} and EL intensity changes during PID-p degradation and recovery processes with corresponding band bending states at the p-Si/AlO_x/SiN_x interfaces (A: Accumulation, B: Depletion, C: Inversion).

EL images performed during positive recovery support this recovery mech-anism and indicate that some cells might not have been in inversion yet after PID-p degradation. In Figure 20, EL images were selected to reflect different stages during recovery for M1, M11 and M35. The top row shows EL images before recovery, the middle row corresponds to EL images when P_{max} is close to its local minimum, and the bottom row shows EL images when P_{max} is increasing (see data points boxed in black in Figure 16). We can distinguish two categories of cells:

- Cells getting darker from the beginning of the recovery to the P_{max} local minium point (1 night of positive bias) and then getting brighter after passing the local minimum (see examples circled in red in Figure 20). These cells were probably in the inversion state after degradation. When the recovery progresses, P_{max} and EL intensity decrease as the Si surface is less and less inverted (state A) before reaching a local minimum when transitioning into depletion (state B) and then increasing as the Si surface is less and less depleted.
- Cells that only get brighter during the recovery process (see examples circled in yellow). These cells were still probably in depletion (state B) after degradation so that the recovery process only consists into improving P_{max} and EL intensity as the Si surface is less and less depleted.

The overall behavior of the modules during recovery will depend on the proportion of cells in depletion and inversion, which can only be clarified through EL measurement. In this case, the vast majority of cells in M1 and M11 were in inversion after PID-p degradation. For M35, most cells seems to only get brighter but it is likely that the initial darkening phase occurs during the first night of positive bias and was not captured by our measurement.

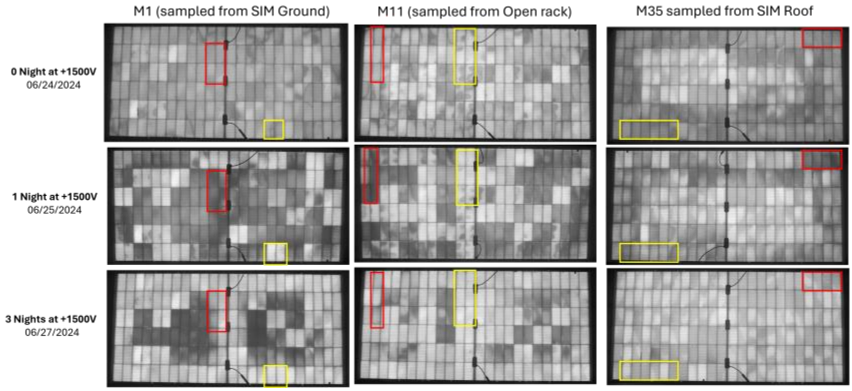

Fig. 20: EL images for M1, M11 and M35 after zero, 1 and 3 nights of positive bias recovery. Images shown are taken on the rear side of the module at name-plate I_{SC}. Cells circled in red are in the inversion state before recovery. Cells circled in yellow are in the local minimum or depletion state before recovery.

4 Conclusion

PID-p was observed in the field on the rear side of bifacial glass/glass *p*-PERC modules for cells negatively-biased at -1500 V and -600 V with respect to the grounded frame. EL images are characterized by a checkerboard pattern attributed to a difference of PID-p susceptibility of the cells within a module. When the -1500 V negative voltage is applied, P_{max} quickly drops the first few days and then stabilizes at ≈ 5% loss when outdoor *I-V* are taken at irradiance above 500 W/m^2 (up to 8% loss at irradiance below 500 W/m^2). Greater degradation rates during the P_{max} dropping phase were reported for increased voltages and wetness on the module surface. A slight impact of the mounting configuration with slower degradation rates when more UV light reaches the modules' backside was also demonstrated. Lower irradiance conditions in fall and winter were correlated with slightly lower P_{max} values. While the front side experienced PID-p in the dark during chamber test, no field degradation was observed due to the important amount of UV light received on the front side of the modules.

Recovery experiments performed on PID-p degraded modules showed a common recovery pattern with P_{max} decreasing to a local minimum before increasing until full recovery. The fastest recovery rates are obtained on modules recovered outdoors with the rear side facing sun, followed by the modules recovered at night under a positive bias, then the modules recovered outdoors with the front side facing the sun. After 1 month of dark storage, P_{max} had dropped but the increasing phase was not observed yet. A relationship between the recovery rate and the total net Coulombs accumulated during degradation was found. When more charge is transferred during degradation (sign of greater PID-p extent), the recovery rate is slower.

A PID-p degradation and recovery mechanism was explained based on the band bending states at the p-Si/AlO_x/SiN_x interfaces: PID-p degradation con-sists of going from accumulation to depletion and eventually inversion with the recovery being a reverse process. This results in a specific power curve shape (clearly observed during recovery) characterized by drop, a local min-imum and an increasing phase. This can be helpful for differentiating PID-p from other minority carrier lifetime-reducing mechanisms and characterizing the relative extent of PID-p-inducing charge that has been transferred during PID-p degradation in the field.

Data availability statement

Reasonable requests for data by email to the authors will be accommodated.

Funding statement

This material is based upon work supported by the U.S. Department of Energy's Office of Energy Efficiency and Renewable Energy (EERE) under the Solar Energy Technologies Office Award Number DE-EE0009345. This work is also part of the SETO Project 38263. This work was authored in part by the National Renewable Energy Laboratory for the U.S. Department of Energy (DOE) under Contract No. DE-AC36-08GO28308. This report was prepared as an account of work sponsored by an agency of the United States Govern-ment. Neither the United States Government nor any agency thereof, nor any of their employees, makes any warranty, express or implied, or assumes any legal liability or responsibility for the accuracy, completeness, or usefulness of any information, apparatus, product, or process disclosed, or represents that its use would not infringe privately owned rights. Reference herein to any specific commercial product, process, or service by trade name, trademark, manufac-turer, or otherwise does not necessarily constitute or imply its endorsement, recommendation, or favoring by the United States Government or any agency thereof. The views and opinions of authors expressed herein do not necessarily state or reflect those of the United States Government or any agency thereof.

Conflicts of interest disclosure

There are no conflicts to declare.

Authors contribution statement

Conceptualization all authors; **Data curation** C. Molto, P. Hacke, D. Colvin, R. Smith, H. Seigneur; Formal analysis C. Molto, P. Hacke, D. Colvin, R. Smith, H. Seigneur; **Funding acquisition** P. Hacke, G. Tamizhmani, and H Seigneur; **Investigation** all authors; **Methodology** all authors; **Project administration** H. Seigneur and C. Molto; **Resources** all authors; **Super-vision** P. Hacke, R. Smith, G. Tamizhmani, and H. Seigneur; **Validation**

all authors; **Visualization** all authors; **Writing - original draft preparation** C. Molto; **Writing - review editing** C.Molto, P.Hacke, F.Li, G. Tamizhmani, J. Oh, R. Smith, and H Seigneur ;

References

[1] Molto, C., Oh, J., Mahmood, F.I., Li, M., Hacke, P., Li, F., Smith, R., Colvin, D., Matam, M., DiRubio, C., Tamizhmani, G., Seigneur, H.: Review of potential-induced degradation in bifacial photovoltaic modules. Energy Technology **11**(4), 2200943 (2023). https://doi.org/10.1002/ente.202200943

[2] Hacke, P., Spataru, S., Habersberger, B., Chen, Y.: Field-representative evaluation of PID-polarization in TOPCon PV modules by accelerated stress testing. Progress in Photovoltaics: Research and Applications **32**(5), 346–355 (2024). https://doi.org/10.1002/pip.3774. Accessed 2024-04-11

[3] Yamaguchi, S., Van Aken, B.B., Masuda, A., Ohdaira, K.: Potential-induced degradation in high-efficiency n-type crystalline-silicon photo-voltaic modules: A literature review. Solar RRL **5**(12), 202100708 (2021). https://doi.org/10.1002/solr.202100708. Accessed 2021-11-05

[4] Yamaguchi, S., Nakamura, K., Masuda, A., Ohdaira, K.: Rapid progression and subsequent saturation of polarization-type potential-induced degradation of n-type front-emitter crystalline-silicon photovoltaic modules. Japanese Journal of Applied Physics **57**(12), 122301 (2018). https://doi.org/10.7567/JJAP.57.122301. Accessed 2021-07-23

[5] Ohdaira, K., Komatsu, Y., Yamaguchi, S., Masuda, A.: Second-stage potential-induced degradation of n-type front-emitter crystalline silicon photovoltaic modules and its recovery. Japanese Journal of Applied Physics (2023). https://doi.org/10.35848/1347-4065/accb60. Accessed 2023-04-17

[6] Carolus, J., Tsanakas, J.A., van der Heide, A., Voroshazi, E., De Ceuninck, W., Daenen, M.: Physics of potential-induced degradation in bifacial p-PERC solar cells. Solar Energy Materials and Solar Cells **200**, 109950 (2019). https://doi.org/10.1016/j.solmat.2019.109950. Accessed 2021-05-25

[7] Hylský, J., Strachala, D., Vyroubal, P., Čudek, P., Vaněk, J., Vanýsek, P.: Effect of negative potential on the extent of PID degradation in photovoltaic power plant in a real operation mode. Microelectronics Reli-ability **85**, 12–18 (2018). https://doi.org/10.1016/j.microrel.2018.04.003. Accessed 2021-05-25

[8] Komatsu, Y., Yamaguchi, S., Masuda, A., Ohdaira, K.: Multistage

performance deterioration in n-type crystalline silicon photovoltaic modules undergoing potential-induced degradation. Microelectronics Reliabil-ity **84**, 127–133 (2018). https://doi.org/10.1016/j.microrel.2018.03.018. Accessed 2021-07-15

[9] Luo, W., Khoo, Y.S., Singh, J.P., Wong, J.K.C., Wang, Y., Aberle, A.G., Ramakrishna, S.: Investigation of Potential-Induced Degradation in n-PERT Bifacial Silicon Photovoltaic Modules with a Glass/Glass Struc-ture. IEEE Journal of Photovoltaics **8**(1), 16–22 (2018). https://doi.org/10.1109/JPHOTOV.2017.2762587. Accessed 2021-07-02

[10] Sporleder, K., Turek, M., Schüler, N., Naumann, V., Hevisov, D., Pöblau, C., Großer, S., Schulte-Huxel, H., Bauer, J., Hagendorf, C.: Quick test for reversible and irreversible PID of bifacial PERC solar cells. Solar Energy Materials and Solar Cells **219**, 110755 (2021). https://doi.org/10.1016/j.solmat.2020.110755. Accessed 2021-05-25

[11] Luo, W., Hacke, P., Terwilliger, K., Liang, T.S., Wang, Y., Ramakrishna, S., Aberle, A.G., Khoo, Y.S.: Elucidating potential-induced degradation in bifacial PERC silicon photovoltaic modules. Progress in Photovoltaics: Research and Applications **26**(10), 859–867 (2018). https://doi.org/10.1002/pip.3028. Accessed 2021-05-25

[12] Carolus, J., Breugelmans, R., Tsanakas, J.A., Heide, A., Voroshazi, E., De Ceuninck, W., Daenen, M.: Why and how to adapt PID testing for bifacial PV modules? Progress in Photovoltaics: Research and Applications **28**(10), 1045–1053 (2020). https://doi.org/10.1002/pip.3311. Accessed 2021-07-02

[13] Yamaguchi, S., Van Aken, B.B., Stodolny, M.K., Löffler, J., Masuda, A., Ohdaira, K.: Effects of passivation configuration and emitter surface doping concentration on polarization-type potential-induced degradation in n-type crystalline-silicon photovoltaic modules. Solar Energy Materials and Solar Cells **226**, 111074 (2021). https://doi.org/10.1016/j.solmat.2021.111074. Accessed 2021-07-14

[14] Hacke, P., Kumar, A., Terwilliger, K., Ndione, P., Spataru, S., Pavgi, A., Choudhury, K.R., Tamizhmani, G.: Evaluation of bifacial module technologies with combined-accelerated stress testing. Progress in Photovoltaics: Research and Applications **31**(12), 1270–1284 (2023). https://doi.org/10.1002/pip.3636. _eprint: https://onlinelibrary.wiley.com/doi/pdf/10.1002/pip.3636. Accessed 2025-07-24

[15] Swanson, R., Cudzinovic, M., DeCeuster, D., Desai, V., Jürgens, J., Kaminar, N., Mulligan, W., Rodrigues-Barbarosa, L., Rose, D., Smith, D.,

Terao, A., Wilson, K.: The surface polarization effect in high-efficiency silicon solar cells. 15th International Photovoltaic Science and Engineering Conference (PVSEC), Shangai, China (2005)

[16] Yamaguchi, S., Masuda, A., Ohdaira, K.: Progression of rapid potential-induced degradation of n-type single-crystalline silicon photovoltaic modules. Applied Physics Express **9**(11), 112301 (2016). https://doi.org/10.7567/APEX.9.112301. Accessed 2021-07-09

[17] Sporleder, K., Naumann, V., Bauer, J., Hevisov, D., Turek, M., Hagen-dorf, C.: Time-Resolved Investigation of Transient Field Effect Passivation States during Potential-Induced Degradation and Recovery of Bifacial Silicon Solar Cells. Solar RRL **5**(7), 2100140 (2021). https://doi.org/10.1002/solr.202100140. Accessed 2021-07-23

[18] Yamaguchi, S., Nakamura, K., Semba, T., Ohdaira, K., Marumoto, K., Ohshita, Y., Masuda, A.: Effects of SiN_x refractive index and SiO_2 thickness on polarization-type potential-induced degradation in front-emitter n-type crystalline-silicon photovoltaic cell modules. Energy Science & Engineering **10**(7), 2268–2275 (2022). https://doi.org/10.1002/ese3.1135. Accessed 2022-11-15

[19] Habersberger, B.M., Hacke, P.: Impact of illumination and encapsulant resistivity on polarization-type potential-induced degradation on n-PERT cells. Progress in Photovoltaics: Research and Applications **30**(5), 455–463 (2021). https://doi.org/10.1002/pip.3505. Accessed 2021-12-29

[20] Oh, K.-s., Bae, S., Lee, K.-j., Kim, D., Chan, S.-i.: Mitigation of potential-induced degradation (PID) based on anti-reflection coating (ARC) structures of PERC solar cells. Microelectronics Reliability **100-101**, 113462 (2019). https://doi.org/10.1016/j.microrel.2019.113462. Accessed 2021-05-25

[21] Janssen, G.J.M., Stodolny, M.K., Van Aken, B.B., Loffler, J., Lamers, M.W.P.E., Tool, K.J.J., Romijn, I.G.: Minimizing the Polarization-Type Potential-Induced Degradation in PV Modules by Modification of the Dielectric Antireflection and Passivation Stack. IEEE Journal of Photovoltaics **9**(3), 608–614 (2019). https://doi.org/10.1109/JPHOTOV.2019.2896944. Accessed 2021-07-02

[22] Luo, W., Hacke, P., Hsian, S.M., Wang, Y., Aberle, A.G., Ramakr-ishna, S., Khoo, Y.S.: Investigation of the Impact of Illumination on the Polarization-Type Potential-Induced Degradation of Crystalline Sil-icon Photovoltaic Modules. IEEE Journal of Photovoltaics **8**(5), 1168–1173 (2018). https://doi.org/10.1109/JPHOTOV.2018.2843791. Accessed 2021-05-25

[23] Sporleder, K., Bauer, J., Groser, S., Richter, S., Hahnel, A., Turek, M., Naumann, V., Ilse, K.K., Hagendorf, C.: Potential-Induced Degradation of Bifacial PERC Solar Cells Under Illumination. IEEE Journal of Photovoltaics **9**(6), 1522–1525 (2019). https://doi.org/10.1109/JPHOTOV.2019.2937231. Accessed 2021-07-07

[24] Xu, Y., Masuda, A., Ohdaira, K.: Influence of light illumination on the potential-induced degradation of n-type interdigitated back-contact crystalline Si photovoltaic modules. Japanese Journal of Applied Physics **60**(SB), 08 (2021). https://doi.org/10.35848/1347-4065/abd9cf. Accessed 2021-09-17

[25] Nguyen, D.C., Ishikawa, Y., Jonai, S., Nakamura, K., Masuda, A., Uraoka, Y.: Elucidating the mechanism of potential induced degradation delay effect by ultraviolet light irradiation for p-type crystalline silicon solar cells. Solar Energy **199**, 55–62 (2020). https://doi.org/10.1016/j.solener.2020.02.034. Accessed 2021-05-25

[26] Jonai, S., Nakamura, K., Masuda, A.: Universal explanation for degradation by charge accumulation in crystalline Si photovoltaic modules with application of high voltage. Applied Physics Express **12**(10), 101003 (2019). https://doi.org/10.7567/1882-0786/ab3cf7. Accessed 2021-07-23

[27] Mahmood, F.I., Li, F., Hacke, P., Molto, C., Colvin, D., Seigneur, H., TamizhMani, G.: Susceptibility to polarization type potential induced degradation in commercial bifacial p-PERC PV modules. Progress in Photovoltaics: Research and Applications **31**(11), 1078–1090 (2023). https://doi.org/10.1002/pip.3724

[28] IEC: Iec 62804-1 photovoltaic (pv) modules – test methods for the detection of potential-induced degradation – part 1: Crystalline silicon. Energy Technology (2015)

[29] Hacke, P., Smith, R., Terwilliger, K., Glick, S., Jordan, D., Johnston, S., Kempe, M., Kurtz, S.: Testing and Analysis for Lifetime Prediction of Crystalline Silicon PV Modules Undergoing Degradation by System Voltage Stress. IEEE Journal of Photovoltaics **3**(1), 246–253 (2013). https://doi.org/10.1109/JPHOTOV.2012.2222351. Accessed 2025-08-04

[30] Hacke, P., Smith, R., Terwilliger, K., Perrin, G., Sekulic, B., Kurtz, S.: Development of an IEC test for crystalline silicon modules to qualify their resistance to system voltage stress. Progress in Photovoltaics: Research and Applications **22**(7), 775–783 (2014). https://doi.org/10.1002/pip.2434. _eprint: https://onlinelibrary.wiley.com/doi/pdf/10.1002/pip.2434. Accessed 2025-08-04

[31] Basak, A., Chakraborty, S., Behura, A.K.: Tilt angle optimization for

bifacial PV module: Balancing direct and reflected irradiance on white painted ground surfaces. Applied Energy **377**, 124525 (2025). https://doi.org/10.1016/j.apenergy.2024.124525. Accessed 2025-12-28

[32] Desharnais, R.: Characterizing the Impact of Potential-Induced Degradation and Recovery on the Irradiance and Temperature Dependence of Photovoltaic Modules. 29th European Photovoltaic Solar Energy Conference and Exhibition; 2346-2350, 5–5468 (2014). https://doi.org/10.4229/EUPVSEC20142014-5CO.14.4. Artwork Size: 5 pages, 5468 kb Medium: application/pdf Publisher: WIP. Accessed 2025-08-04

[33] Golive, Y.R., Kottantharayil, A., Vasi, J., Shiradkar, N.: Determining the optimal standard test condition correction procedure for high-throughput field $I - V$ measurements of photovoltaic modules. Progress in Photovoltaics: Research and Applications **30**(1), 13–26 (2022). https://doi.org/10.1002/pip.3457. Accessed 2025-08-04

[34] Hacke, P., Molto, C., Colvin, D., Smith, R., Mahmood, F.I., Li, F., Oh, J., Tamizhmani, G., Seigneur, H.: Polarization-type potential-induced degradation in bifacial PERC modules in the field. EPJ Photovoltaics **16**, 16 (2025). https://doi.org/10.1051/epjpv/2025004. Accessed 2025-02-26

[35] Aberle, A.G., Glunz, S., Warta, W.: Impact of illumination level and oxide parameters on Shockley–Read–Hall recombination at the Si-SiO2 interface. Journal of Applied Physics **71**(9), 4422–4431 (1992). https://doi.org/10.1063/1.350782. Accessed 2025-08-07